ISSN 0454－4641

運輸省港湾技術研究所

港湾技術研究所報告

REPORT OF THE PORT AND HARBOUR RESEARCH INSTITUTE

MINISTRY OF TRANSPORT

VOL.39 NO.4 Dec. 2000

NAGASE, YOKOSUKA, JAPAN

港湾技術研究所報告（REPORT OF P. H. R. I.）
第 39 巻　第 4 号（Vol. 39, No. 4），　2000年12月（Dec. 2000）

目　　次（CONTENTS）

REPORT OF THE PORT AND
HARBOUR RESEARCH INSTITUTE
Vol.39 No.4 (Dec. 2000)

A Boussinesq Model to Study Long Period Waves in a Harbor

Md. Hasanat ZAMAN*
Katsuya HIRAYAMA**
Tetsuya HIRAISHI***

Synopsis

This work shows the possibility and extend of using a Boussinesq type wave model for the simulation of long period waves those encroach a harbor. The basic physics of this model follows the description of Madsen and Sørensen (1992) that uses the concept of depth averaged velocity distribution with enhanced dispersion characteristics. A finite difference method has been employed for the numerical computation that follows ADI algorithm. As an application of the model we have considered Nakada harbor of Okinawa Prefecture. This port sometimes suffers from the unusual wave hazards and results into great disturbances in ship handling. The navigation channel inside the harbor is recently dredged to 5m water depth while in some places in the close vicinity the depth is around 1m. So the bottom contour plays a vital role over the wave evolution in this region. Extensive field observation have been done at three different locations of which two are inside and the rest is located at well outside of the harbor towards the offshore direction. Field observations performed from the beginning of October 1999 to middle of December 1999. For this particular study we have chosen few cases from the above three months. The observed data at the offshore location have been used as the incident boundary conditions for the model. Later we have compared the simulated and observed results at the two other locations inside the harbor. The simulated results show fairly great agreement with the observed data.

Keywords: Boussinesq model, Long period wave, Field data, Harbor

* Visiting Scientist of Wave Laboratory, Hydraulic Engineering Division

** Research Engineer of Wave Laboratory, Hydraulic Engineering Division

*** Chief of Wave Laboratory, Hydraulic Engineering Division

(3-1-1 Nagase, Yokosuka, Kanagawa, Japan 239-0826

Tel: +81-468- 44-5063, Fax: +81-468-41-3888, e-mail: zaman@cc.phri.go.jp)

港湾技術研究所報告
第39巻第4号(2000.12)

ブシネスクモデルを用いた港内長周期波の計算

エムディ. ハサナット ジャーマン* ・ 平山克也** ・ 平石哲也***

要 旨

風波を対象とした高精度な波浪変形計算を行う手法として，近年，ブシネスク方程式に基づいた波浪変形計算モデルの開発が盛んに行われている．これらの研究では，浅海波に対してブシネスク方程式を適用することを目的として，モデル方程式の線形分散特性の改良，あるいは近似精度の向上などの試みがなされている．これは，ブシネスク方程式の導出過程において，流速の鉛直分布に長波近似を導入して鉛直積分されていることに起因しており，この意味で，本来，ブシネスク方程式は長波を対象とした波動方程式であるといえる．

本研究で対象とした港湾は沖縄県の仲田港である．本港湾では，1999年10月から同年12月の期間に港口部および港内で観測された現地データの解析結果より，港内に周期30秒から300秒程度の長周期波が存在することが認められた．また本港湾は，港内に発達した珊瑚礁を有するため，浚渫により水深５ｍの航路が確保される一方，その他の水域では，ところによっては水深が１ｍ程度となる個所があるなど，非常に水深変化に富んだ地形的特質を有している．したがって本港湾における波浪変形計算では，長波の伝播に対して高い計算精度が期待され，かつ波の回折や反射のみならず屈折や浅水変形が考慮されるブシネスクモデルを用いることが適切であると判断された．

そこで本研究では，Madsen and Sørensen (1992) によるブシネスクモデルを用いて，実際に現地で観測されたいくつかの長周期波を対象とした波浪変形計算を行い，３地点で観測された現地データとの比較より，その計算精度を検証した．港口部で観測された時間波形のうち，周期30秒以上の時間波形を抽出してモデルに入射させたところ，計算モデルによって港内で得られる時間波形は，現地観測により得られた各地点の時間波形をよく再現していることが確認された．

キーワード：ブシネスクモデル，長周期波，現地観測，港湾

---

*水工部波浪研究室客員研究員
**水工部波浪研究室
***水工部波浪研究室長
239-0826 神奈川県横須賀市長瀬3-1-1
Tel: +81-468-44-5063, Fax: +81-468-41-3888, e-mail: zaman@cc.phri.go.jp

CONTENTS

1. Introduction

Long period wave is well known in imparting considerable difficulties to the port facilities. Both in normal and catastrophic situation they can cause huge damages to the anchored ships, mooring systems and other port facilities and, thus may affect the overall port efficiency. In the recent years there is an upsurge of using Boussinesq equation based numerical models to study the nearshore hydrodynamic processes. This is because it has been reported by many researchers that the approximation done by the recent Boussinesq models agree well with the relevant physical experiments and field observations. The major aptness of such models is they can be useful to study the wave transformation including breaking (Svendsen et al., 1996) for wide range of area from deep sea to swash zone (Sørensen et. al., 1996) with well-nigh confidence. Essentially ocean wave field contains waves of different heights, frequencies and directions. The wave field is transformed and it experiences a lot of changes into its basic feature when it moves towards coast from the offshore region due to change of water depth. A large number of researchers have been extending their effort to bring such model into most attractive form. Peregrine (1967), Abbotts et al. (1978), Flaten and Rygg (1991), Madsen and Sørensen (1991), Sato et al. (1992), Karambas and Koutitas (1992), Nwogu (1993), Hiraishi et al., (1995), Madsen et al (1997a and 1997b), Bayram and Larson (2000) are some of them.

In this study a Boussinesq equation based numerical model has been developed and employed for the computation of transformed long waves inside a harbor. The basic physics of this model follows the description of Madsen and Sørensen (1992). An enhanced dispersion relation has been invoked in the simulation. As an application we have applied our model to study the long period wave field in Nakada harbor of Okinawa Prefecture in Japan.

Nakada is the only port in Izena town of Okinawa Prefecture of Japan. The town Izena is in an isolated island and presently waterway serves as the only mode of public transportation to and from the main cities of Okinawa. Two large breakwaters protect this port from the East Side. The bottom topography in and around this harbor is not uniform. The navigation channel inside the harbor is recently dredged to 5m water depth where the depth at the entrance is about 10m. The entrance and the close vicinity of this harbor have considerable coral reefs. This port sometimes experiences unusual wave hazards that create great uncertainty in port management. The Local Government of Okinawa Prefecture has given great attention to find out the reason of such problem in order to take necessary counter measures. In this connection they have managed to collect field data at three different locations in and well outside the harbor. Initially we have analyzed these data and observed considerable presence of long period wave that is usually known to create problems to the port facility.

Our primary interest is to track the available long period waves. Considering the frequency distribution and respective amplitude in the power spectrum obtained from the field data we have chosen the waves of period 30s to 300s from the collected data sets for this study. Later simulated results are compared with the observed field data.

2. Basic Formulation

The wave transformation model used in this study is based on the Boussinesq equations with improved dispersion characteristics as reported by Madsen et al. (1991) and Madsen and Sørensen (1992). The basic continuity equation and equation of motions for x and y directions can be read as follows:

$$\eta_t + P_x + Q_y = 0 \tag{1}$$

$$P_t + \left(P^2/D\right)_x + \left(PQ/D\right)_y + gD\eta_x + \varepsilon P + \frac{f}{2D^2} P\sqrt{P^2+Q^2} = \nu\left(P_{xx} + P_{yy}\right) + \left(B+\frac{1}{3}\right)h^2\left(P_{xxt} + Q_{xyt}\right) + Bah^3\left(\eta_{xxx} + \eta_{xyy}\right) + hh_x\left(\frac{1}{3}P_{xt} + \frac{1}{6}Q_{yt}\right) + hh_y\left(\frac{1}{6}Q_{yt}\right) + Bgh^2\left[h_x\left(2\eta_{xx} + \eta_{yy}\right) + h_y\eta_{xy}\right] \quad (2)$$

$$Q_t + \left(PQ/D\right)_x + \left(Q^2/D\right)_y + gD\eta_y + \varepsilon Q + \frac{f}{2D^2} Q\sqrt{P^2+Q^2} = \nu\left(Q_{xx} + Q_{yy}\right) + \left(B+\frac{1}{3}\right)h^2\left(Q_{yyt} + P_{xyt}\right) + Bah^3\left(\eta_{yyy} + \eta_{xxy}\right) + hh_y\left(\frac{1}{3}Q_{yt} + \frac{1}{6}P_{xt}\right) + hh_x\left(\frac{1}{6}P_{yt}\right) + Bgh^2\left[h_y\left(2\eta_{yy} + \eta_{xx}\right) + h_x\eta_{xy}\right] \quad (3)$$

where η is the instantaneous water surface elevation, P the depth integrated velocity component (flux) in the x-direction, Q the depth integrated velocity component (flux) in the y-direction, h the local still water depth, D ($=h+\eta$) the local instantaneous water depth, g the gravitational acceleration, ε the boundary dumping function varies linearly along the width of the sponge layers and null elsewhere, ν the eddy viscosity describes the momentum exchange due to turbulence, f the energy dissipation coefficient and the subscripts x, y and t denote the differentiation with respect to space and time. The parameter B is an important factor in the dispersion relation that depreciates the computational error in the wave celerity and group velocity.

The expression for ν can be given in the following way (Sato *et al.*, 1992 and Bayram and Larson, 2000):

$$\nu = \frac{\alpha_D g d \tan\delta}{\sigma^2}\sqrt{\frac{g}{d}\frac{\hat{Q}-Q_r}{Q_s-Q_r}} \quad (4)$$

in which α_D is a coefficient (2.5 in the surf zone and null elsewhere), $\tan\delta$ the bottom slope, d the mean water depth and σ is the angular frequency. $\hat{Q}$ is the flow amplitude, Q_s the wave induced flow inside the surf zone and Q_r is the flow amplitude of the reform waves and are expressed as follows:

$$Q_s = 0.4(0.57 + 5.3\tan\delta)\sqrt{gd^3} \quad (5)$$

$$Q_r = 0.135\sqrt{gd^3} \quad (6)$$

The wave number would be evaluated from the following dispersion relation in which B is equal to 1/15 corresponds to the frequency dispersion obtained from Padé's (2,2) expansion of the Stokes first-order theory.

$$\frac{c^2}{gh} = \frac{1 + Bk^2h^2}{1 + (B+\frac{1}{3})k^2h^2} \quad (7)$$

where k is the wave number and c is the wave celerity.

A simple comparison between the linear dispersion relation and the one obtained from Padé's approximation is shown in **Figure 1**.

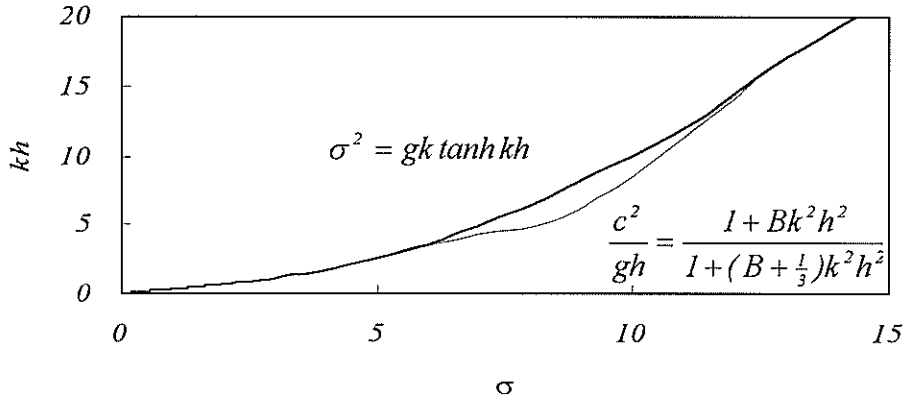

Fig. 1 Comparison between dispersion relations

From the above figure it may be observed that for a particular range of angular frequencies (σ) the dispersion relation obtained from the small-amplitude wave theory, underscores the wavelength.

3. Numerical Model

A Finite difference numerical method has been employed for the solution of the governing equations. The discretization is done following the mesh shown in **Figure 2**. The above governing equations have been discretized in such a way so that the solution could be obtained by ADI algorithm. The discretized equations are shown in the Appendix.

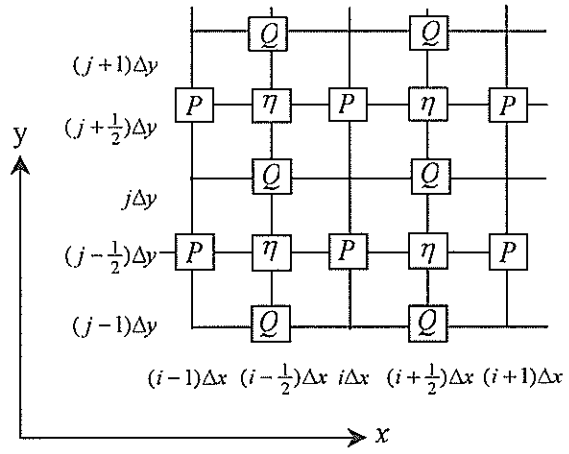

Fig. 2 Computational mesh

4. Application of the Model

As an application the obtained model has been applied to study the long period waves in the Nakada harbor of Okinawa Prefecture. An overview of Nakada harbor is shown in **Figure 3**. This figure also shows the locations of the observation stations.

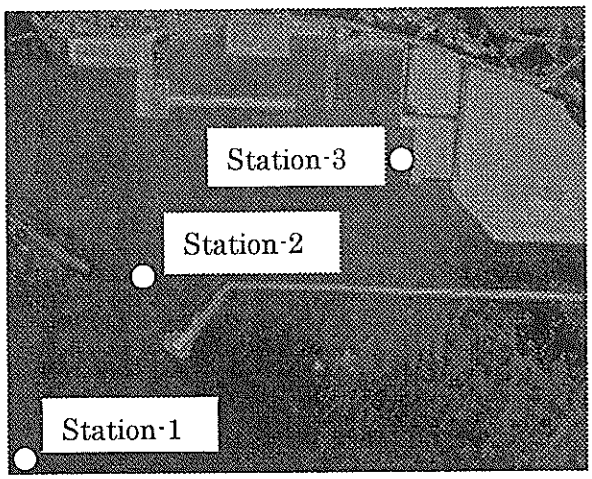

Fig. 3 An overview of Nakada harbor
Station-1 [(26°55'11", 127°57'43"), *h*=24.2m], Station-2 [(26°55'13", 127°57'23"), *h*=10.3m] and, Station-3 [(26°55'24", 127°57'18"), *h*=5.5m]

4.1 Computational Conditions

Three sets of data have been chosen from the observed data for this study. In all cases observed data at Station-1 have been used as the incident boundary conditions for the numerical model. The basic characteristics of these wave-sets at Station-1 are shown in **Table 1**.

Table 1 [SI unit] ODS1 (Original Data Station-1), C1 (Case-1, etc.)

ODS1	YY	MM	DD	Hours	Depth	Significant		Dir.
						$H_{1/3}$	$T_{1/3}$	
C1	99	10	25	14~18	24.22	1.41	7.30	E
C2	99	11	29	06~08	24.23	0.97	7.00	E
C3	99	12	11	02~04	24.13	0.51	8.10	E

As an example, **Figures 4(a)** and **4(b)** respectively show the surface elevation and energy distribution for the data of ODS1C1.

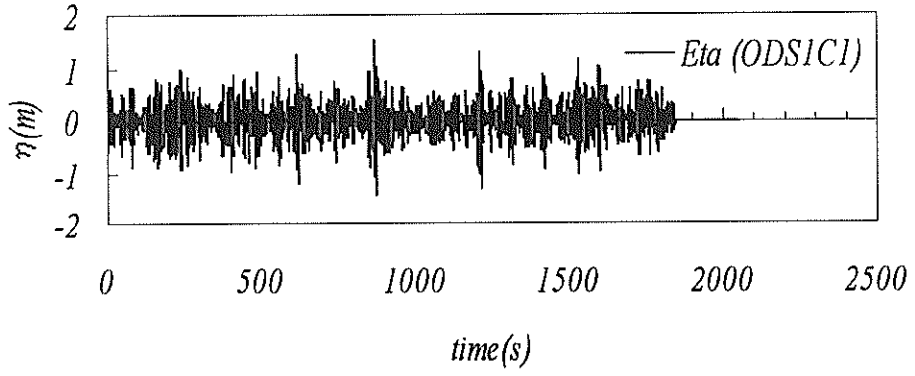

Fig. 4(a) Instantaneous surface elevation for ODS1C1

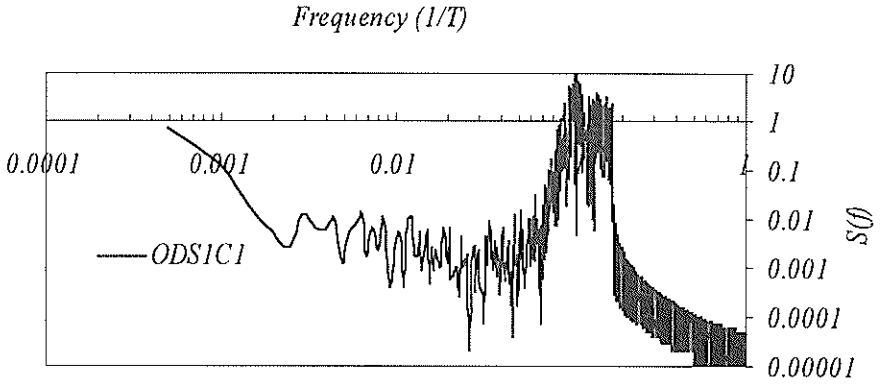

Fig. 4(b) Energy distribution for ODS1C1

From these figures we have assumed that waves having periods in between 30s to 300s would serve our purpose since we are interested to examine the long period waves in the harbor. Rest two cases ODS1C2 and ODS1C3 are considered in the similar fashion. An inverse Fourier transformation method is adopted to isolate the waves having period 30s to 300s from the original data sets. **Table 2** shows the extracted waves parameters and these parameters are later used as the incident boundary condition for the numerical simulation. In all cases wave directions and phases are computed from the observed current velocities in the *x-y* plane and surface elevation data, respectively.

Table 2 [SI unit] EDS1 (Extracted Data Station-1); Wave period: 30s~300s

EDS1	YY	MM	DD	Hours	Depth	Significant		Dir.
						$H_{1/3}$	$T_{1/3}$	
C1	99	10	25	14~18	24.22	0.033	89.86	E24°N
C2	99	11	29	06~08	24.23	0.017	84.43	E8°S
C3	99	12	11	02~04	24.13	0.013	75.94	E8°N

Figure 5(a) shows the extracted surface elevation data in the range of 30s to 300s, on the other hand, **Figure 5(b)** describes their contribution to gross energy.

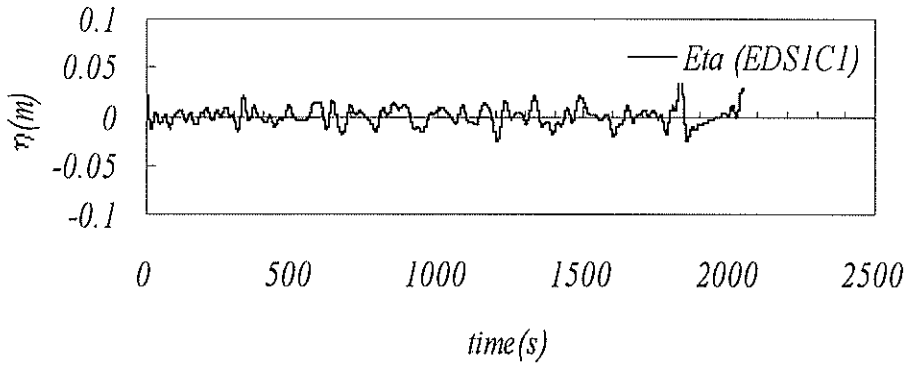

Fig. 5(a) Instantaneous surface elevation for EDS1C1

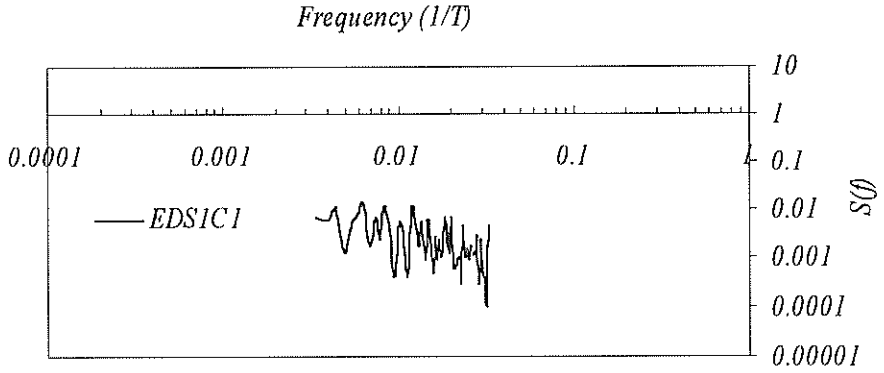

Fig. 5(b) Energy distribution for EDS1C1

4.2 Adjustment of Reflection Coefficient

Usually long period waves inherit considerable reflection. Numerically a sponge layer having a width equivalent to twice of the incoming wavelength or more can absorb most of the wave energies. But physically this job is still neither easy nor economic for a long period wave. In this study we have considered waves in the range of 30s to 300s. From the field survey we have assumed that a 90% reflection may be occurred in the case of the above wave range. Energy dumping event in a sponge layer follows the following relation:

$$\varepsilon_j = \frac{\gamma \varepsilon_m}{2(\sinh\gamma - \gamma)}\left[\cosh(\gamma X_j / F) - 1\right] \quad ; \quad j = 1, 2 \tag{8}$$

where the term ε_j is the boundary damping function and is null elsewhere apart from the boundary, $\varepsilon_m = \sqrt{gh}$, γ is a coefficient, F is the width of the sponge layer and X_j is the horizontal distance along the sponge layer in the x and y directions, respectively.

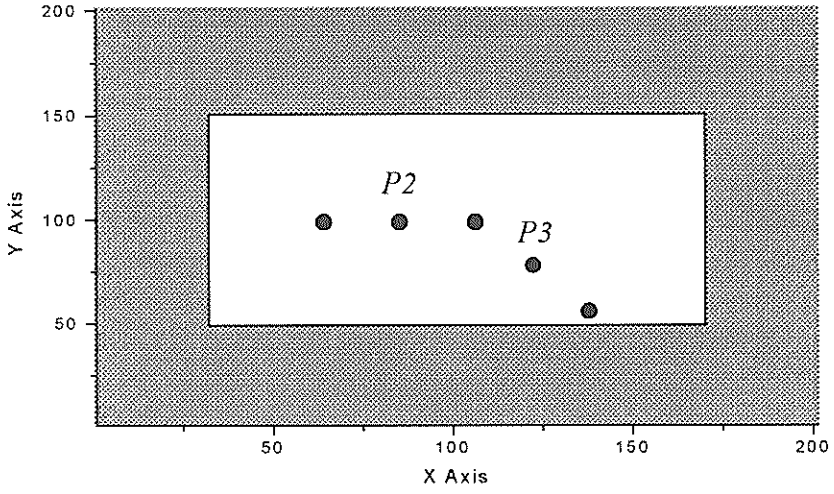

Fig. 6(a) Computational domain for reflection coefficient (not to the scale)

Our approach is to find out a reasonable value of γ to be used for a sponge layer with a width which is essentially less than a half of the incoming wavelength and reflects about 90% of the wave energy. To do that we have used Eq. 8 and checked it out for varying γ. The computational domain for this case is shown in **Figure 6(a)**. In this computation a

uniform water depth of 10m is assumed over the whole domain. From **Table 2** it may be observed that the significant wave periods for all the cases is close to 90s. So a regular wave train of 10cm wave height, 90s wave period, and a sponge layer of width 400m have been used in this particular study.

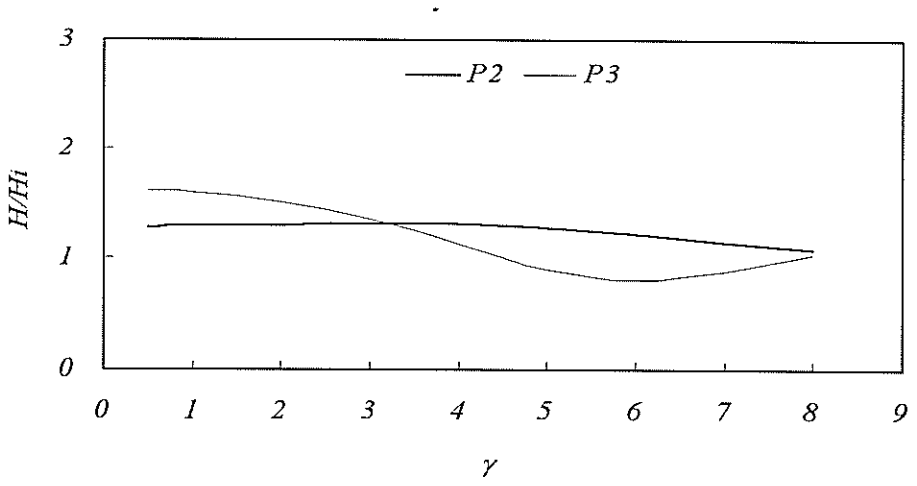

Fig. 6(b) Effect of γ in energy dumping

From **Figure 6(b)** it may be perceived that a value of γ is 3 should serve our purpose. In the above figure it may be observed that when γ takes a value of 8 the sponge layer used here is able to dump almost all the energies at locations *P2* and *P3*.

5. Results and Discussions

We have mentioned in **Table 1** that ODS1C1, ODS1C2 and ODS1C3 represent the original observed data at Station-1 in three different months, days and hours, respectively, on the other hand, in **Table 2**, EDS1C1, EDS1C2 and EDS1C3 express their corresponding extracted data in the range of 30s to 300s wave period. Similarly EDS2C1, EDS2C2 and EDS2C3 describe the corresponding extracted wave at Station-2 and, EDS3C1, EDS3C2 and EDS3C3 stand for Station-3. The original and extracted data at Station-2 and Station-3 are not shown here separately but are used in the comparisons.

5.1 Linear Solution

In general the second order flux-related terms in the momentum equations are discarded in the long period wave approximation because of the smallness in the wave steepness. It is known that the dispersion characteristics of a wave field in a shallow water region are more significant than a deep-water wave and a linear model can not reproduce the dispersive characteristics of a wave field as like as a nonlinear model. On the other hand, a high-order Boussinesq model, because of its structure and formulation, contains a number of higher order derivatives those considerably affect the computational effort when the flux-related terms are not even active. So it is worthy to mention here that a linearized Boussinesq model does not curtail the computational time significantly as well. In this computation we have linearized our Boussinesq model and then as a test case, a unidirectional irregular wave field having significant wave height 0.75m, significant wave period 12s and uniform water depth of 10m with a 400 nos. of wave components have been adopted for simulation. Later the obtained results are compared with the corresponding nonlinear solution. It is expected that overall results obtain from both the linear and nonlinear model may not vary significantly but obviously there will be fundamental differences. **Figures 7(a)** and **7(b)** show the comparisons of the surface elevations obtained from a linear and a nonlinear solution at Station-2 and Station-3, respectively. In this study we have used the non-linear model as it is.

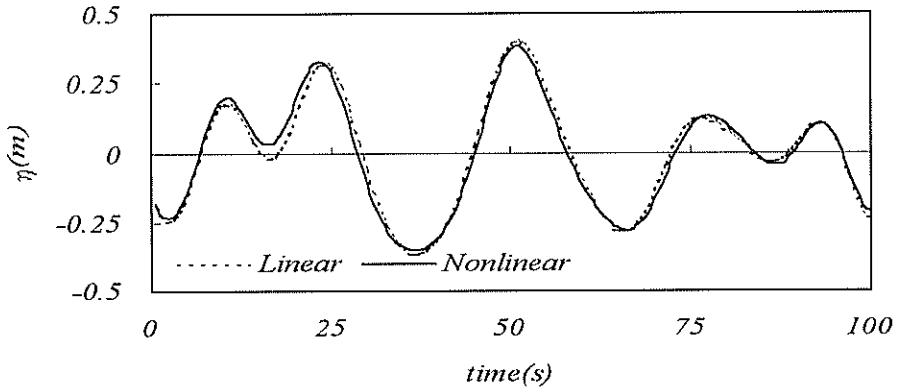

Fig. 7(a) Comparisons of surface elevations between linear and nonlinear solution at Station-2

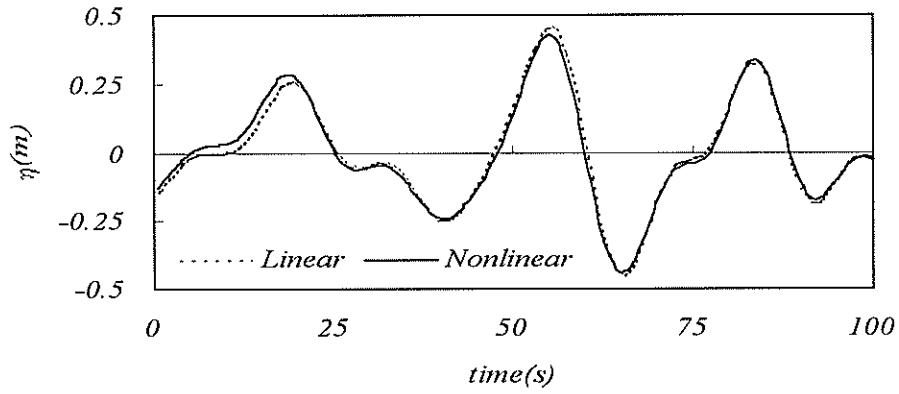

Fig. 7(b) Comparisons of surface elevations between linear and nonlinear solution at Station-3

5.2 Nonlinear Solution

In the simulation EDS1C1, EDS1C2 and EDS1C3 have been utilized as the incident wave conditions for the model. **Figures 8(a)** and **8(b)** show the comparisons of the surface elevations and energy distributions between simulated wave and the respective observed wave at Station-2 for EDS2C1 while **Figures 8(c)** and **8(d)** demonstrate their coherency and phase difference.

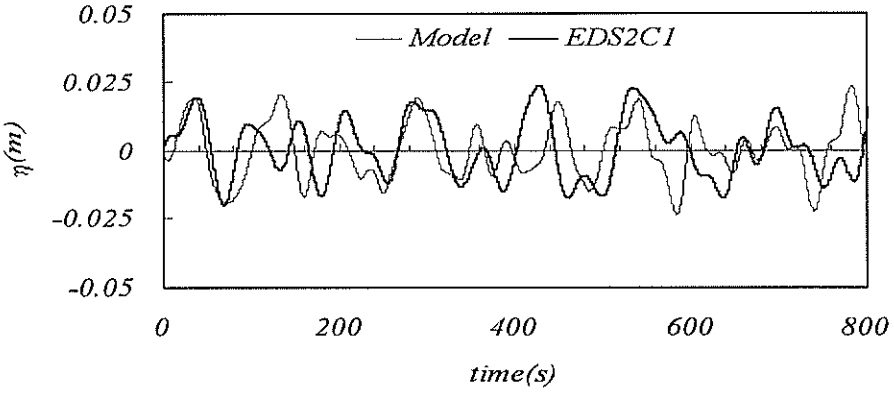

Fig. 8(a) Comparisons of surface elevations at Station-2 for EDS2C1

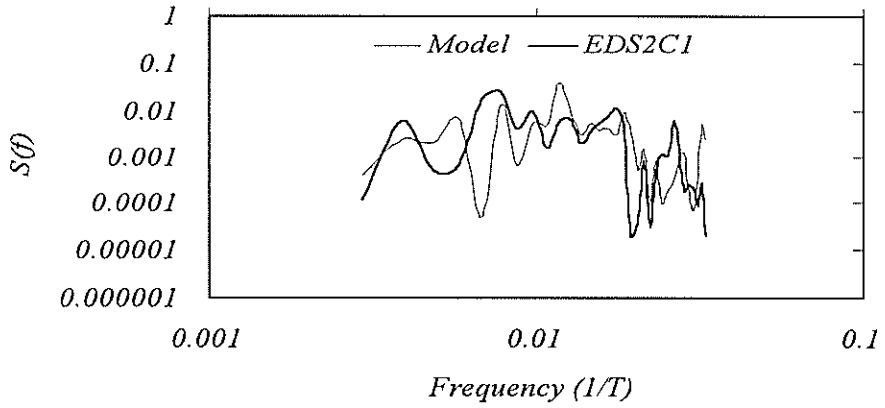

Fig. 8(b) Comparisons of energy distributions at Station-2 for EDS2C1

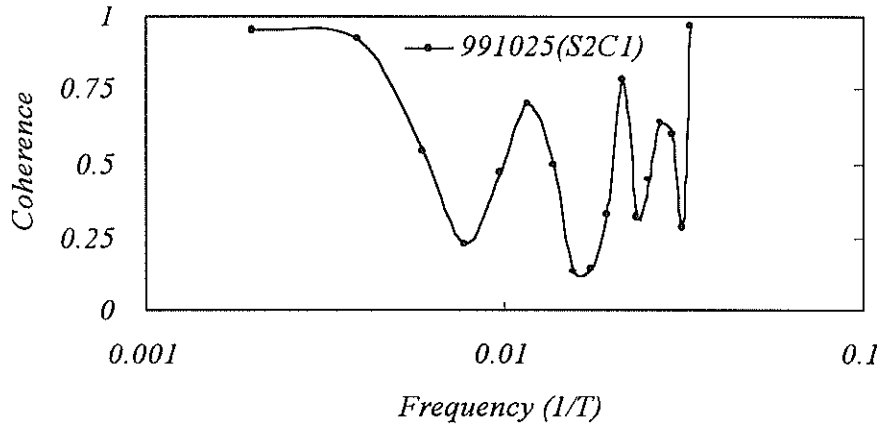

Fig. 8(c) Coherency at Station-2 for EDS2C1

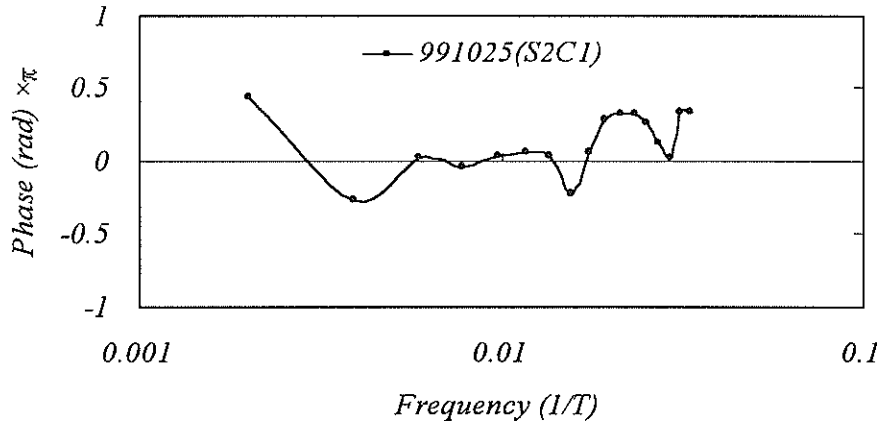

Fig. 8(d) Phase difference at Station-2 for EDS2C1

Figures 9(a) and **9(b)** compare the surface elevations and energy distributions of simulated and observed wave at

Station-2 for EDS2C2 while **Figures 9(c)** and **9(d)** represent their coherency and phase difference.

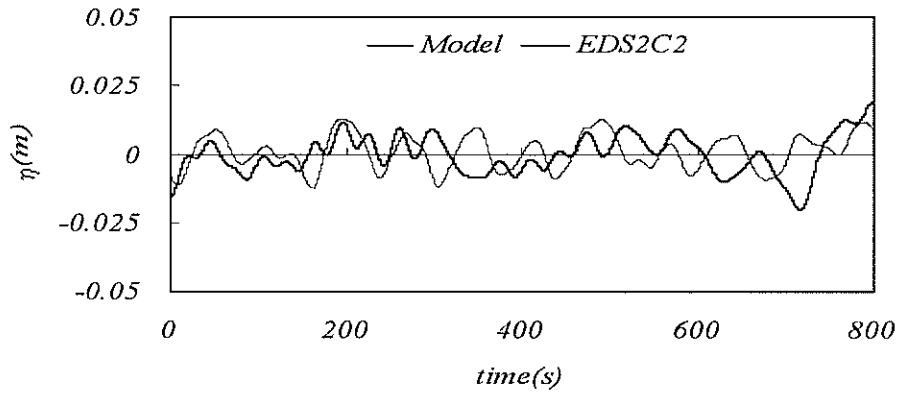

Fig. 9(a) Comparisons of surface elevations at Station-2 for EDS2C2

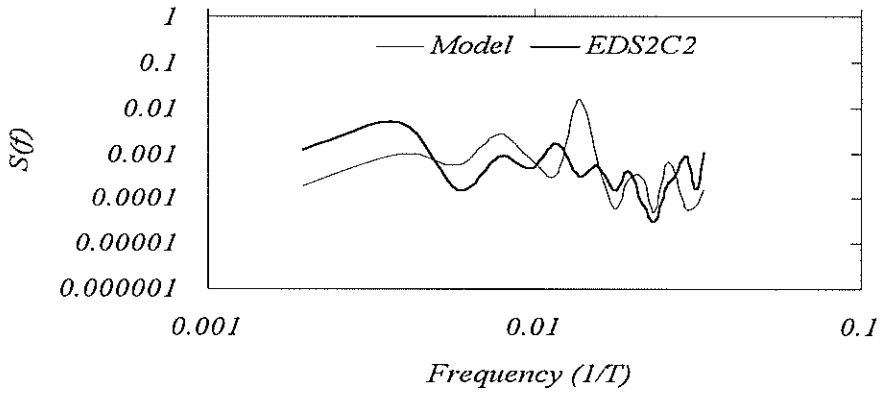

Fig. 9(b) Comparisons of energy distributions at Station-2 for EDS2C2

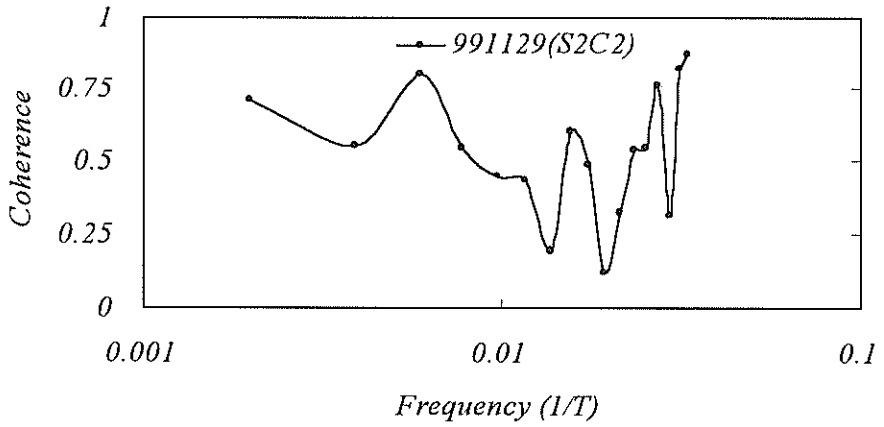

Fig. 9(c) Coherency at Station-2 for EDS2C2

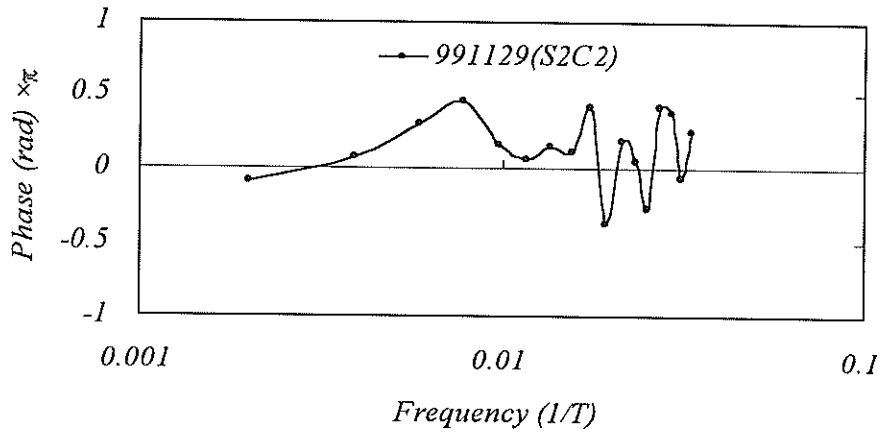

Fig. 9(d) Phase difference at Station-2 for EDS2C2

Figures 10(a) and **10(b)** show the contrast of the surface elevations and energy distributions of the simulated and observed wave at Station-2 for EDS2C3 while **Figures 10(c)** and **10(d)** specify their coherency and phase difference.

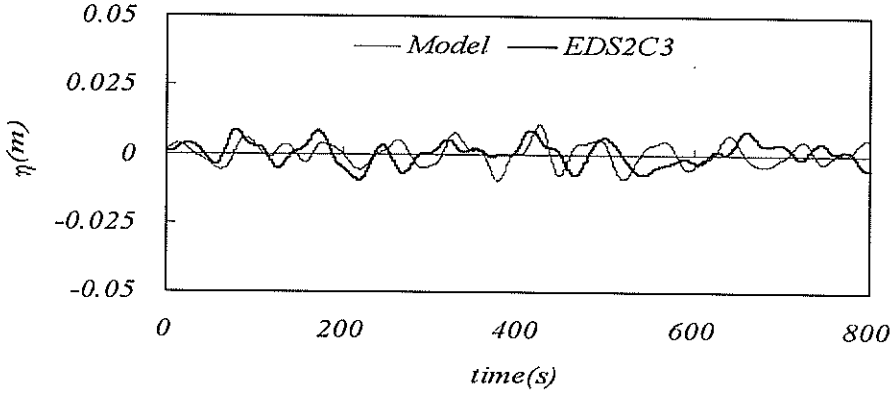

Fig. 10(a) Comparisons of surface elevations at Station-2 for EDS2C3

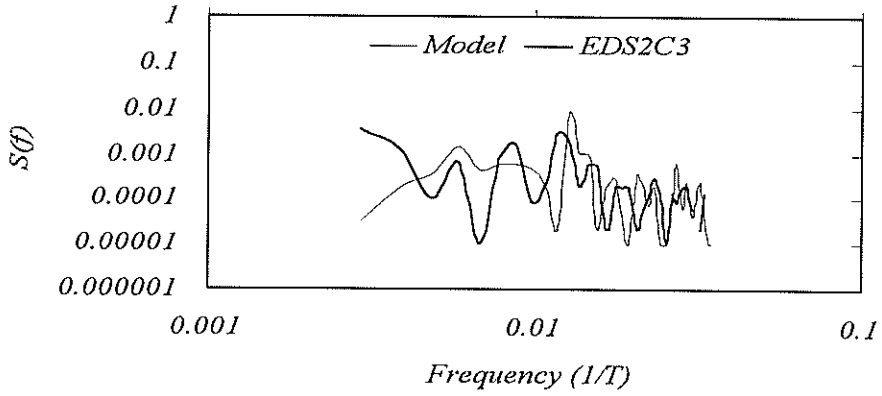

Fig. 10(b) Comparisons of energy distributions at Station-2 for EDS2C3

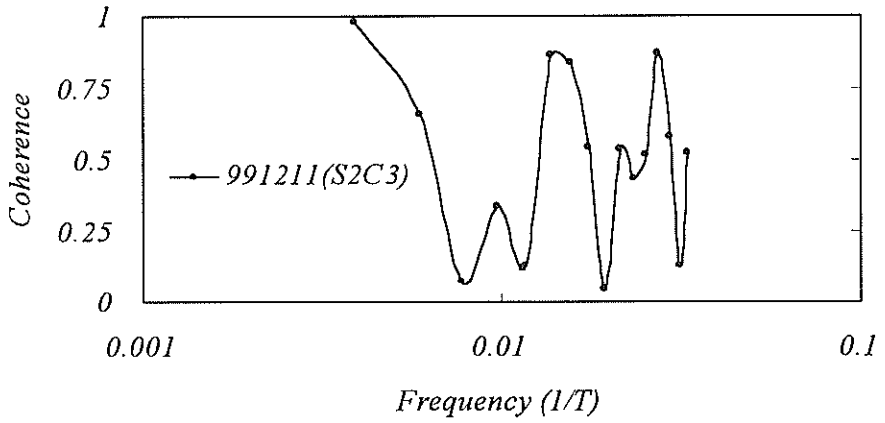

Fig. 10(c) Coherency at Station-2 for EDS2C3

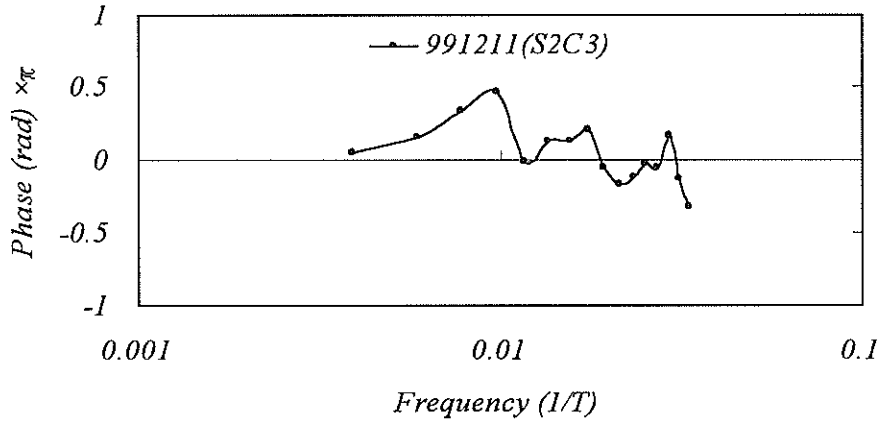

Fig. 10(d) Phase difference at Station-2 for EDS2C3

Figures 11(a) and **11(b)** represent the comparisons of the surface elevations and energy distributions obtained from the model and from the field observation at Station-3 for EDS3C1 while **Figures 11(c)** and **11(d)** account their coherency and phase difference.

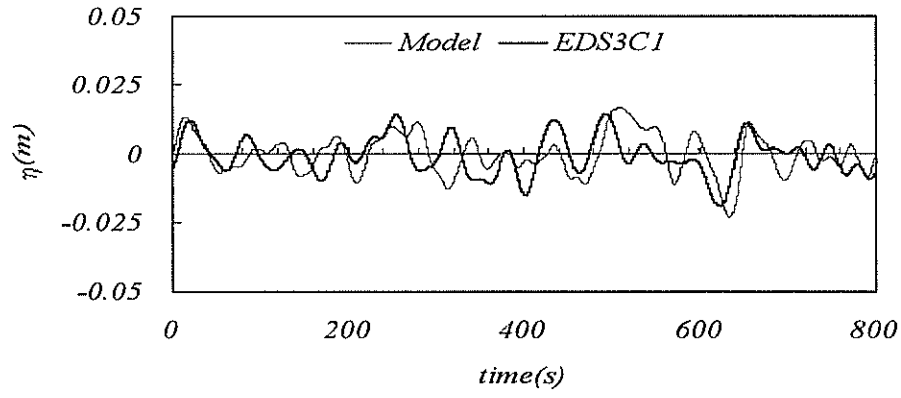

Fig. 11(a) Comparisons of surface elevations at Station-3 for EDS3C1

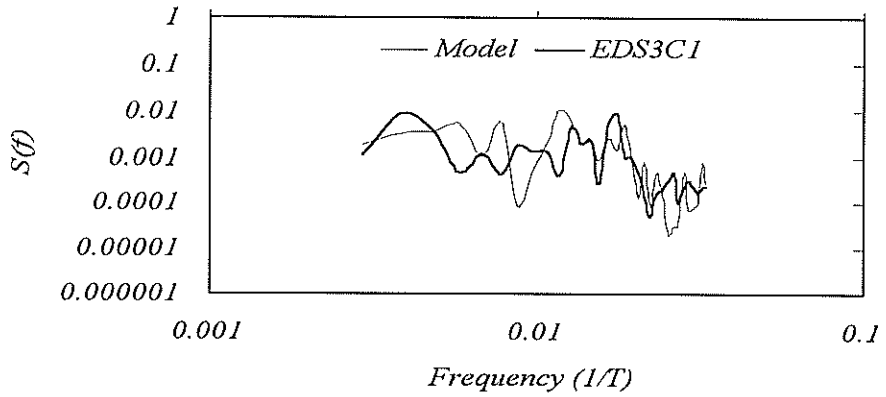

Fig. 11(b) Comparisons of energy distributions at Station-3 for EDS3C1

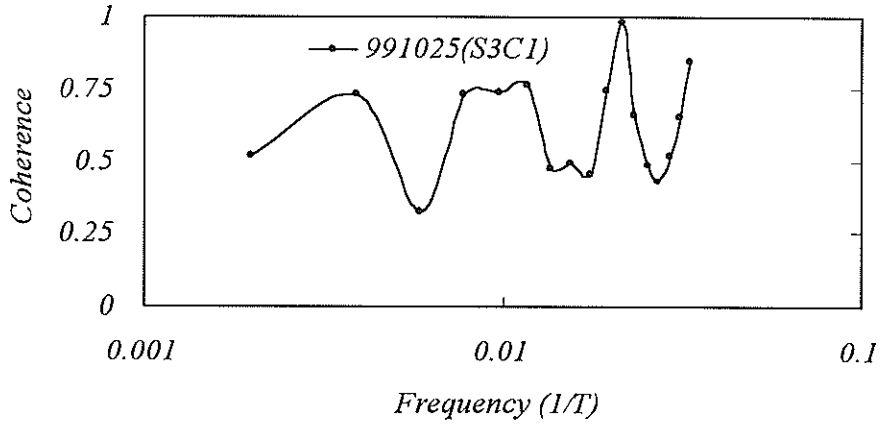

Fig. 11(c) Coherency at Station-3 for EDS3C1

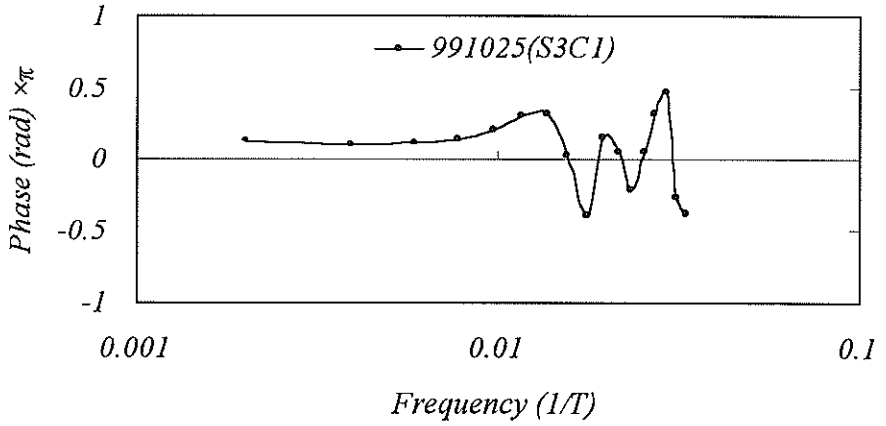

Fig. 11(d) Phase difference at Station-3 for EDS3C1

Figures 12(a) and **12(b)** symbolize the contrast of the surface elevations and energy distributions of the simulated

and the relevant observed wave at Station-3 for EDS3C2 while **Figures 12(c)** and **12(d)** describe their coherency and phase difference.

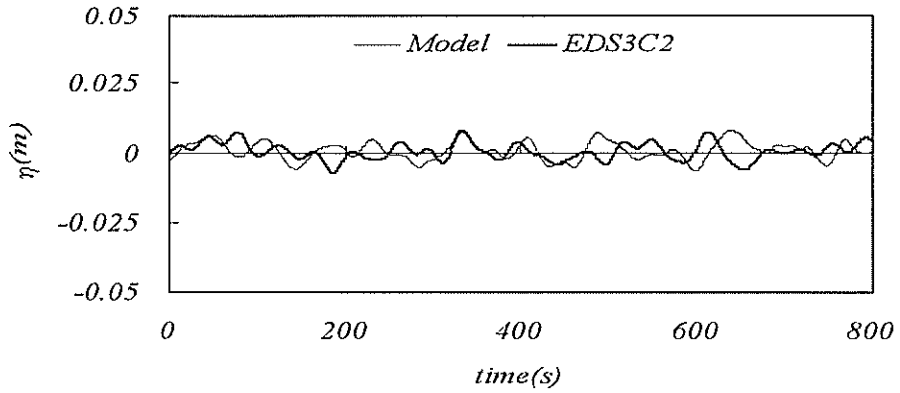

Fig. 12(a) Comparisons of surface elevations at Station-3 for EDS3C2

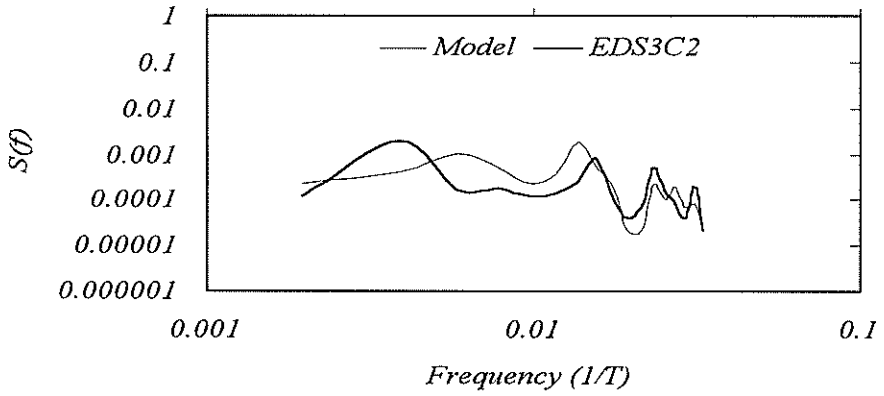

Fig. 12(b) Comparisons of energy distributions at Station-3 for EDS3C2

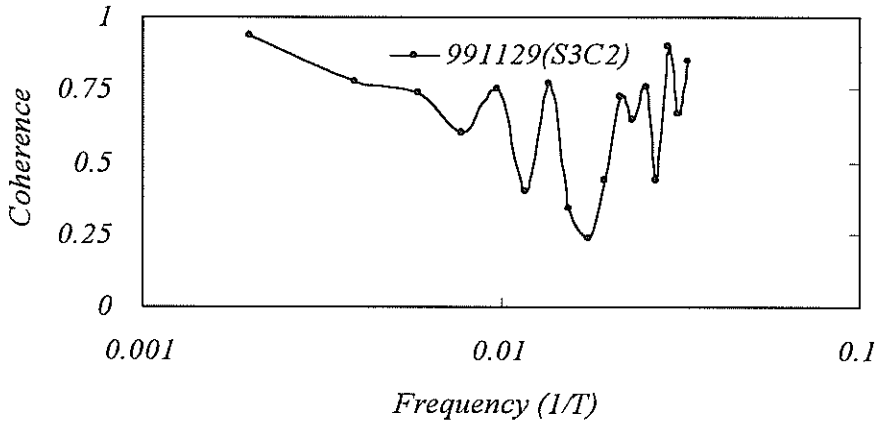

Fig. 12(c) Coherency at Station-3 for EDS3C2

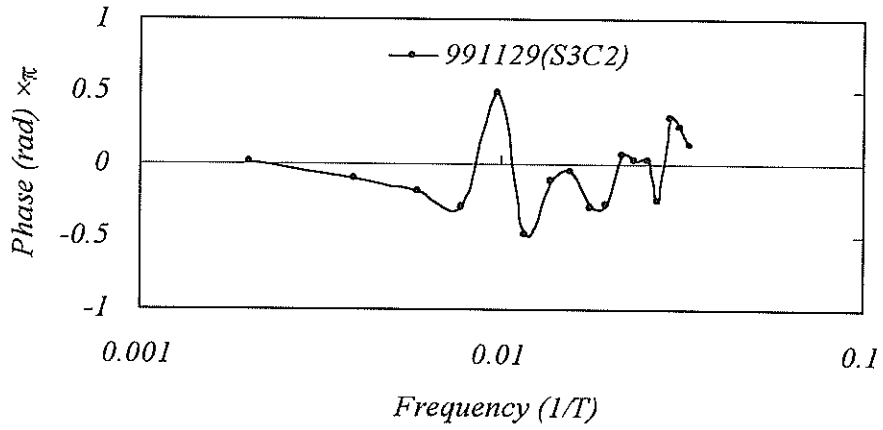

Fig. 12(d) Phase difference at Station-3 for EDS3C2

Figures 13(a) and **13(b)** portray the comparisons of the surface elevations and energy distributions of the simulated and the corresponding observed data at Station-3 for EDS3C3 while **Figures 13(c)** and **13(d)** illustrate their coherency and phase difference.

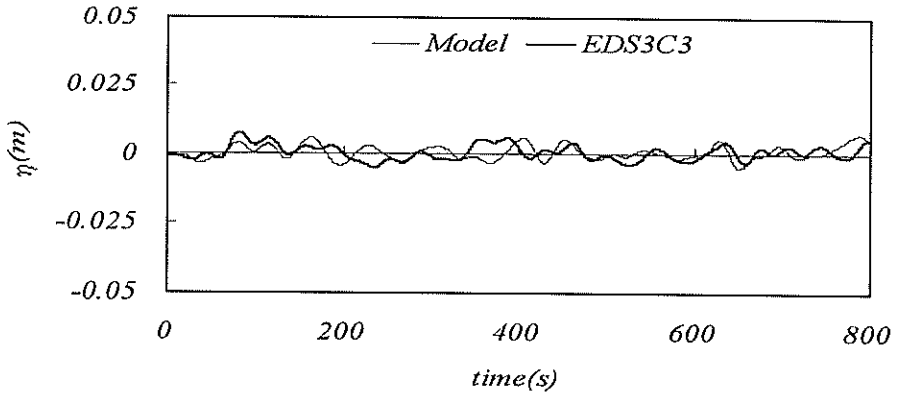

Fig. 13(a) Comparisons of surface elevations at Station-3 for EDS3C3

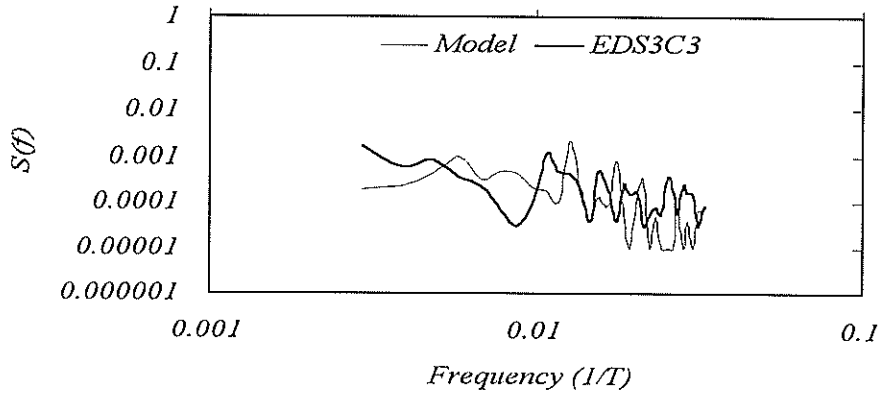

Fig. 13(b) Comparisons of energy distributions at Station-3 for EDS3C3

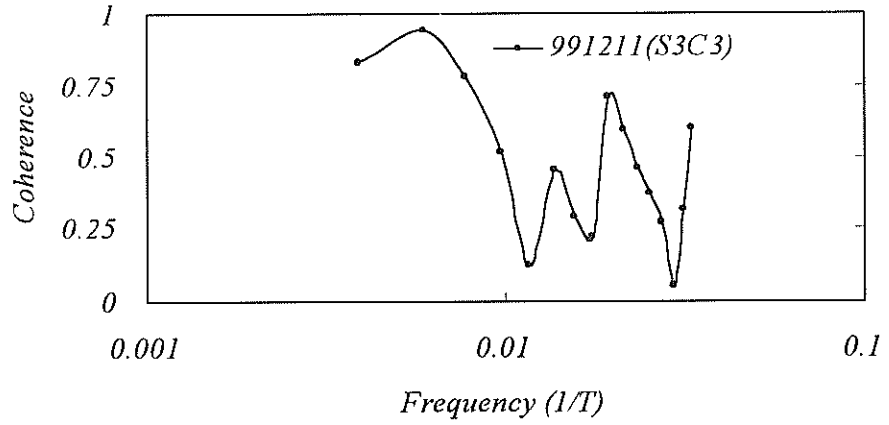

Fig. 13(c) Coherency at Station-3 for EDS3C3

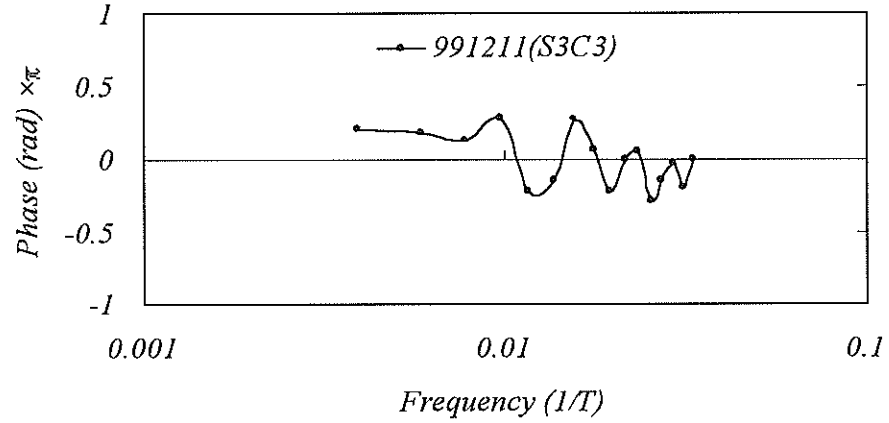

Fig. 13(d) Phase difference at Station-3 for EDS3C3

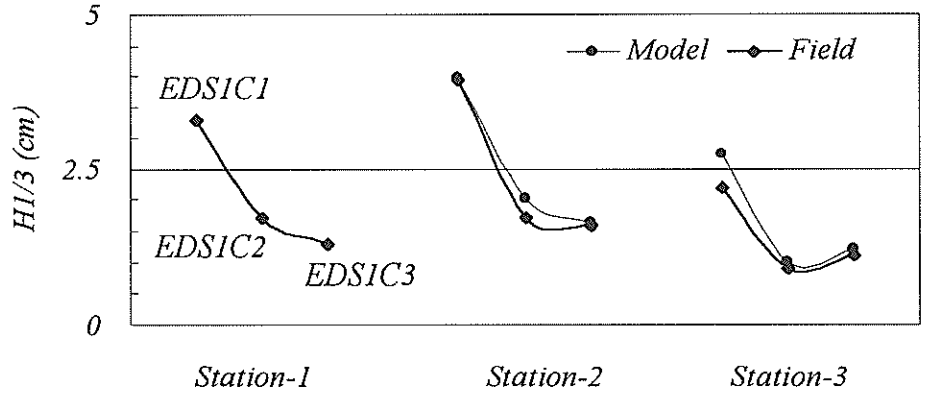

Fig. 14 Observed wave heights at Station-1 and comparisons of their corresponding obserbed and simulated wave heights at Station-2 and Station-3

Figure 14 displays the incident wave heights observed at Station-1 and comparisons between computed and observed significant wave heights for the above three cases at Station-2 and Station-3.

From **Figures 8(a)**, **9(a)**, **10(a)**, **11(a)**, **12(a)**, and **13(a)** it may be perceived that computed instantaneous surface elevations agree pretty well with the observed data at both the stations inside the harbor for the above three cases. These observations are well supported by the **Figure 14** where comparisons between the computed and observed significant wave heights are found to match each other to a large extent at the both measuring stations.

6. Conclusions

A nonlinear two-dimensional Boussinesq model with enhanced dispersion characteristics has been examined to study the long period waves in a harbor. In this study observed data in Nakada harbor of Okinawa Prefecture have been utilized. Three sets of data of different months, days and times are considered. In all the cases observed data at the offshore station (Station-1) have been used as the incident boundary conditions for the model. Later we have compared the simulated and observed results at the other two stations (Station-2 and Station 3) inside the harbor. Comparisons are carried out for instantaneous surface elevation, energy distribution, coherence and phase difference. The simulated results show fairly great agreement with the observed data. Some initial results show that for the case of any provisional estimation a linearized model may be used but a nonlinear model is desirable for the enhancement of the accuracy in the results. This model might be a useful tool to reconfigure the Nakada harbor for possible safty though we believe that this model is applicable more generally.

(Received on August 31, 2000)

References

Abbott, M. B., H. M. Petersen and O. Skovgaard (1978): On the numerical modelling of short waves in shallow water, *Journal of Hydraulic Research*, 16(3), pp.173-204

Bayram, A. and M. Larson (2000): Wave transformation in the nearshore zone: comparison between a Boussinesq model and field data, *Coastal Engineering*, Elsevier, 39, pp.149-171

Flaten, G. and O.B. Rygg (1991): Dispersive shallow water waves over a porous sea bed, *Coastal Engineering*, Elsevier, 15, pp.347-369

Hiraishi, T., I. Uehara and Y. Suzuki (1995): Applicability of wave transformation model in Boussinesq equations, *Report of the Port and Harbor Research Institute*, Japan, No.814, pp.1-22

Karambas, TH. V. and C. Koutitas (1992): A breaking wave propagation model based on Boussinesq equations, *Coastal Engineering*, Elsevier, 18, pp.1-19

Madsen, P.A., O.R. Sørensen and H.A. Schäffer (1997a): Surf zone dynamics simulated by a Boussinesq type model: Part:I. Model description and cross-shore motion of regular waves, *Coastal Engineering*, Elsevier, 32, pp.255-287

Madsen, P.A., O.R. Sørensen and H.A. Schäffer (1997b): Surf zone dynamics simulated by a Boussinesq type model: Part:II. Surf beat and swash oscillations for wave groups and irregular waves, *Coastal Engineering*, Elsevier, 32, pp.289-319

Madsen, P.A. and O.R. Sørensen (1992): A new form of Boussinesq equations with improved linear dispersion characteristics, Part 2. A slowly varying bathymetry, *Coastal Engineering*, Elsevier, 18, pp.183-204.

Nwogu, O. (1993): An alternating form of the Boussinesq equations for modelling the propagation of waves from deep to shallow water, *Journal of waterway, port and coastal and ocean engineering*, 1196, pp.618-638

Peregrine, G. H.(1967): Long wave on a beach, *Journal of Fluid Mechanics*, Vol:27, Part:4, pp.715-827

Sato, S., M. Kabiling and H. Suzuki (1992): Prediction of near bottom velocity history by a non-linear dispersive wave model, *Coastal Engineering in Japan*, 35(1), pp.68-82

Sørensen, O.R., P.A. Madsen and H.A. Schäffer (1996): Nonlinear wave dynamics in the surf zone, *Proc. 25th Coast. Eng. Conf*, ASCE, pp.1178-1191

Svendsen, I. A., K. Yu and J. Veeramony (1996): A Boussinesq breaking wave model with vorticity, *Proc. 25th Coast. Eng. Conf*, ASCE, pp.1192-1204

List of Symbols

The following symbols are used in the present paper:

B	:	dispersion parameter
c	:	wave celerity
d	:	mean water depth
D	:	instantaneous local water depth ($h+\eta$)
f	:	frictional cofficient
F	:	width of the sponge layer
g	:	acceleration due to gravity
h	:	still water depth
H	:	local wave height
H_i	:	incident wave height
$H_{1/3}$	:	significant wave height
i	:	x-grid point
j	:	y-grid point
k	:	wave number
n	:	computational time step
P, P_t	:	fluxes in the x-direction
Q, Q_t	:	fluxes in the y-direction
$\hat{Q}$	:	flow amplitude
Q_s	:	scattered the flow amplitude
Q_r	:	flow amplitude of the reformed wave
$S(f)$	:	frequency spectrum
t	:	time
T	:	wave period
x	:	horizontal axis
X_j	:	distances in the sponge layer for x and y direction
α_D	:	a coefficient
δ	:	bottom slope
η	:	surface fluctuation
γ	:	sponge layer related coefficient
ν	:	eddy viscosity
σ	:	angular frequency
ε_j	:	boundary-damping function in the x and y direction
ε_m	:	damping coefficient

Appendix

After discretization the X-direction continuity and momentum equations take the following forms:

$$\frac{2\left(\eta_{i+1/2,j+1/2}^{n+1/2}-\eta_{i+1/2,j+1/2}^{n}\right)}{\Delta t}+\frac{1}{2}\left(\frac{P_{i+1,j+1/2}^{n+1}-P_{1,j+1/2}^{n+1}}{\Delta x}+\frac{P_{i+1,j+1/2}^{n}-P_{i,j+1/2}^{n}}{\Delta x}\right)$$

$$+\frac{1}{2}\left(\frac{Q_{i+1/2,j+1}^{n+1/2}-Q_{i+1/2,j}^{n+1/2}}{\Delta y}+\frac{Q_{i+1/2,j+1}^{n-1/2}-Q_{i+1/2,j}^{n-1/2}}{\Delta y}\right)=0$$

$$\frac{P_{i,j+1/2}^{n+1}-P_{i,j+1/2}^{n}}{\Delta t}$$

$$+\frac{1}{4\Delta x}\left[\frac{\left(P_{i,j+1/2}^{n+1}+P_{i+1,j+1/2}^{n+1}\right)\left(P_{i,j+1/2}^{n}+P_{i+1,j+1/2}^{n}\right)}{D_{i+1/2,j+1/2}^{*}}-\frac{\left(P_{i,j+1/2}^{n+1}+P_{i+1,j+1/2}^{n+1}\right)\left(P_{i,j+1/2}^{n}+P_{i+1,j+1/2}^{n}\right)}{D_{i-1/2,j+1/2}^{*}}\right]$$

$$+\frac{1}{4\Delta y}\left[\frac{\left(P_{i,j+1/2}^{n+1}+P_{i,j+3/2}^{n}\right)\left(Q_{i-1/2,j+1}^{n+1/2}+Q_{i+1/2,j+1}^{n+1/2}\right)}{D_{i,j+1}^{*}}-\frac{\left(P_{i,j+1/2}^{n+1}+P_{i,j-1/2}^{n}\right)\left(Q_{i-1/2,j}^{n+1/2}+Q_{i+1/2,j}^{n+1/2}\right)}{D_{i,j}^{*}}\right]$$

$$+gD_{i,j+1/2}^{*}\frac{\left(\eta_{i+1/2,j+1/2}^{n+1/2}-\eta_{i-1/2,j+1/2}^{n+1/2}\right)}{\Delta x}$$

$$-\frac{1}{2}\nu_{i,j+1/2}\left[\frac{P_{i+1,j+1/2}^{n+1}-2P_{i,j+1/2}^{n+1}+P_{i-1,j+1/2}^{n+1}}{(\Delta x)^2}+\frac{P_{i+1,j+1/2}^{n}-2P_{i,j+1/2}^{n}+P_{i-1,j+1/2}^{n}}{(\Delta x)^2}\right]$$

$$-\nu_{i,j+1/2}\left[\frac{P_{i,j+3/2}^{n}-2P_{i,j+1/2}^{n}+P_{i,j-1/2}^{n}}{(\Delta x)^2}\right]+\frac{1}{2}\varepsilon_{i,j+1/2}\left(P_{i,j+1/2}^{n+1}+P_{i,j+1/2}^{n}\right)$$

$$+\frac{1}{4}\frac{f}{\left(D_{i,j+1/2}^{*}\right)^2}\left(P_{i,j+1/2}^{n+1}+P_{i,j+1/2}^{n}\right)\sqrt{\left(P_{i,j+1/2}^{n}\right)^2+\left(\bar{\bar{Q}}_{i,j+1/2}^{n+1/2}\right)^2}$$

$$=C_{Bht}^{x}\left[\frac{\left(P_{i+1,j+1/2}^{n+1}-2P_{i,j+1/2}^{n+1}+P_{i-1,j+1/2}^{n+1}\right)-\left(P_{i+1,j+1/2}^{n}-2P_{i,j+1/2}^{n}+P_{i-1,j+1/2}^{n}\right)}{(\Delta x)^2}\right]$$

$$+C_{Bht}^{x}\left[\frac{\left(Q_{i+1/2,j+1}^{n+1/2}-Q_{i-1/2,j+1}^{n+1/2}-Q_{i+1/2,j}^{n+1/2}+Q_{i-1/2,j}^{n+1/2}\right)-\left(Q_{i+1/2,j+1}^{n+1/2}-Q_{i-1/2,j+1}^{n+1/2}-Q_{i+1/2,j}^{n+1/2}+Q_{i-1/2,j}^{n+1/2}\right)}{\Delta x\Delta y}\right]$$

$$+Bg\,\bar{h}_{i,j+1/2}^{-x^3}\left[\frac{\eta_{i+3/2,j+1/2}^{*}-3\eta_{i+1/2,j+1/2}^{*}+3\eta_{i-1/2,j+1/2}^{*}-\eta_{i-3/2,j+1/2}^{*}}{(\Delta x)^3}\right]$$

$$+Bg\,\bar{h}_{i,j+1/2}^{-x^3}\left[\frac{\eta_{i+1/2,j+3/2}^{*}-2\eta_{i+1/2,j+1/2}^{*}+\eta_{i+1/2,j-1/2}^{*}}{\Delta x(\Delta y)^2}\right]$$

$$- Bg \overset{-x}{h}{}^{3}_{i,j+1/2}\left[\frac{\eta^{*}_{i-1/2,j+3/2} - 2\eta^{*}_{i-1/2,j+1/2} + \eta^{*}_{i-1/2,j-1/2}}{\Delta x(\Delta y)^2}\right]$$

$$+ \frac{\overset{-x}{h}_{i,j+1/2}\left(h_{i+1/2,j+1/2} - h_{i-1/2,j+1/2}\right)}{\Delta t \Delta x}\left[\frac{1}{6}\frac{\left(P^{n+1}_{i+1,j+1/2} - P^{n+1}_{i-1,j+1/2}\right) - \left(P^{n}_{i+1,j+1/2} - P^{n}_{i-1,j+1/2}\right)}{\Delta x}\right]$$

$$+ \frac{\overset{-x}{h}_{i,j+1/2}\left(h_{i+1/2,j+1/2} - h_{i-1/2,j+1/2}\right)}{\Delta t \Delta x}\left[\frac{1}{6}\frac{\left(\overset{-x}{Q}{}^{n+1/2}_{i,j+1} - \overset{-x}{Q}{}^{n+1/2}_{i,j}\right) - \left(\overset{-x}{Q}{}^{n-1/2}_{i,j+1} - \overset{-x}{Q}{}^{n-1/2}_{i,j}\right)}{\Delta y}\right]$$

$$+ \frac{\overset{-x}{h}_{i,j+1/2}\left(\overset{=}{h}_{i,j+1} - \overset{=}{h}_{i,j}\right)}{\Delta t \Delta x}\left[\frac{1}{6}\frac{\left(\overset{-y}{Q}{}^{n+1/2}_{i+1/2,j+1/2} - \overset{-y}{Q}{}^{n+1/2}_{i-1/2,j+1/2}\right) - \left(\overset{-y}{Q}{}^{n-1/2}_{i+1/2,j+1/2} - \overset{-y}{Q}{}^{n-1/2}_{i-1/2,j+1/2}\right)}{\Delta y}\right]$$

$$+ Bg \overset{-x}{h}{}^{2}_{i,j+1/2}\left[2\frac{\left(h_{i+1/2,j+1/2} - h_{i-1/2,j+1/2}\right)}{\Delta x}\frac{\left(\overset{-x}{\eta}{}^{*}_{i+1,j+1/2} - 2\overset{-x}{\eta}{}^{*}_{i,j+1/2} + \overset{-x}{\eta}{}^{*}_{i-1,j+1/2}\right)}{(\Delta x)^2}\right]$$

$$+ Bg \overset{-x}{h}{}^{2}_{i,j+1/2}\left[\frac{\left(h_{i+1/2,j+1/2} - h_{i-1/2,j+1/2}\right)}{\Delta x}\frac{\left(\overset{-x}{\eta}{}^{*}_{i,j+3/2} - 2\overset{-x}{\eta}{}^{*}_{i,j+1/2} + \overset{-x}{\eta}{}^{*}_{i,j-1/2}\right)}{(\Delta y)^2}\right]$$

$$+ Bg \overset{-x}{h}{}^{2}_{i,j+1/2}\left[2\frac{\left(\overset{=}{h}_{i,j+1} - \overset{=}{h}_{i,j}\right)}{\Delta y}\frac{\left(\overset{-y}{\eta}{}^{*}_{i+1/2,j+1} - \overset{-y}{\eta}{}^{*}_{i-1/2,j+1} - \overset{-y}{\eta}{}^{*}_{i+1/2,j} + \overset{-y}{\eta}{}^{*}_{i-1/2,j}\right)}{\Delta x \Delta y}\right]$$

where,

$$C^{x}_{Bht} = \left(B + \frac{1}{3}\right)\frac{\overset{-x}{h}{}^{2}_{i,j+1/2}}{\Delta t}$$

$$D^{*}_{i,j+1/2} = \overset{-x}{h}_{i,j+1/2} + \overset{-x}{\eta}{}^{*}_{i,j+1/2}$$

$$D^{*}_{i+1/2,j+1/2} = h_{i+1/2,j+1/2} + \eta^{*}_{i+1/2,j+1/2}$$

$$D^{*}_{i-1/2,j+1/2} = h_{i-1/2,j+1/2} + \eta^{*}_{i-1/2,j+1/2}$$

$$D^{*}_{i,j+1} = \overset{=}{h}_{i,j+1} + \overset{=}{\eta}{}^{*}_{i,j+1}$$

$$D^*_{i,j} = \bar{h}_{i,j} + \bar{\eta}^*_{i,j}$$

After discretization the *Y*-direction continuity and momentum equations take the following forms:

$$\frac{2\left(\eta^{n+1}_{i+1/2,j+1/2} - \eta^{n+1/2}_{i+1/2,j+1/2}\right)}{\Delta t} + \frac{1}{2}\left(\frac{Q^{n+3/2}_{i+1/2,j+1} - Q^{n+3/2}_{i+1/2,j}}{\Delta y} + \frac{Q^{n+1/2}_{i+1/2,j+1} - Q^{n+1/2}_{i+1/2,j}}{\Delta y}\right)$$

$$+ \frac{1}{2}\left(\frac{P^{n+1}_{i+1,j+1/2} - P^{n+1}_{i,j+1/2}}{\Delta x} + \frac{P^{n}_{i+1,j+1/2} - P^{n}_{i,j+1/2}}{\Delta x}\right) = 0$$

$$\frac{Q^{n+3/2}_{i+1/2,j} - Q^{n+1/2}_{i+1/2,j}}{\Delta t}$$

$$+ \frac{1}{4\Delta y}\left[\frac{\left(Q^{n+3/2}_{i+1/2,j} + Q^{n+3/2}_{i+1/2,j+1}\right)\left(Q^{n+1/2}_{i+1/2,j} + Q^{n+1/2}_{i+1/2,j+1}\right)}{D^{**}_{i+1/2,j+1/2}} - \frac{\left(Q^{n+3/2}_{i+1/2,j} + Q^{n+3/2}_{i+1/2,j-1}\right)\left(Q^{n+1/2}_{i+1/2,j} + Q^{n+1/2}_{i+1/2,j-1}\right)}{D^{**}_{i+1/2,j-1/2}}\right]$$

$$+ \frac{1}{4\Delta x}\left[\frac{\left(Q^{n+3/2}_{i+1/2,j} + Q^{n+1/2}_{i+3/2,j}\right)\left(P^{n+1}_{i+1,j-1/2} + P^{n+1}_{i+1,j+1/2}\right)}{D^{**}_{i,j+1}} - \frac{\left(Q^{n+3/2}_{i+1/2,j} + Q^{n+1/2}_{i-1/2,j}\right)\left(P^{n+1}_{i,j-1/2} + P^{n+1/2}_{i,j+1/2}\right)}{D^{**}_{i,j}}\right]$$

$$+ gD^{**}_{i+1/2,j}\frac{\left(\eta^{n+1}_{i+1/2,j+1/2} - \eta^{n+1}_{i+1/2,j-1/2}\right)}{\Delta x}$$

$$- \frac{1}{2}\nu_{i+1/2,j}\left[\frac{Q^{n+3/2}_{i+1/2,j+1} - 2Q^{n+3/2}_{i+1/2,j} + Q^{n+3/2}_{i+1/2,j-1}}{(\Delta y)^2} + \frac{Q^{n+1/2}_{i+1/2,j+1} - 2Q^{n+1/2}_{i+1/2,j} + Q^{n+1/2}_{i+1/2,j-1}}{(\Delta y)^2}\right]$$

$$- \nu_{i+1/2,j}\left[\frac{Q^{n+1/2}_{i+3/2,j} - 2Q^{n+1/2}_{i+1/2,j} + Q^{n+1/2}_{i-1/2,j}}{(\Delta x)^2}\right] + \frac{1}{2}\varepsilon_{i+1/2,j}\left(Q^{n+3/2}_{i+1/2,j} + Q^{n+1/2}_{i+1/2,j}\right)$$

$$+ \frac{1}{4}\frac{f}{\left(D^{**}_{i+1/2,j}\right)}\left(Q^{n+3/2}_{i/1/2,j} + Q^{n+1/2}_{i+1/2,j}\right)\sqrt{\left(Q^{n+1/2}_{i+1/2,j}\right)^2 + \left(\bar{P}^{n+1}_{i+1/2,j}\right)^2}$$

$$= C^{y}_{Bht}\left[\frac{\left(Q^{n+3/2}_{i+1/2,j+1} - 2Q^{n+3/2}_{i+1/2,j} + Q^{n+3/2}_{i+1/2,j-1}\right) - \left(Q^{n+1/2}_{i+1/2,j+1} - 2Q^{n+1/2}_{i+1/2,j} + Q^{n+1/2}_{i+1/2,j-1}\right)}{(\Delta y)^2}\right]$$

$$+ C^{y}_{Bht}\left[\frac{\left(P^{n+1}_{i+1,j+1/2} - P^{n+1}_{i,j+1/2} - P^{n+1}_{i+1,j-1/2} + P^{n+1}_{i,j-1/2}\right) - \left(P^{n}_{i+1,j+1/2} - P^{n}_{i,j+1/2} - P^{n}_{i+1,j-1/2} + P^{n}_{i,j-1/2}\right)}{\Delta x \Delta y}\right]$$

$$+ Bg\,\bar{h}^{-y^3}_{i+1/2,j}\left[\frac{\eta^{**}_{i+1/2,j+3/2} - 3\eta^{**}_{i+1/2,j+1/2} + 3\eta^{**}_{i+1/2,j-1/2} - \eta^{**}_{i+1/2,j-3/2}}{(\Delta y)^3}\right]$$

$$+ Bg\,\bar{h}^{-y^3}_{i+1/2,j}\left[\frac{\eta^{**}_{i+3/2,j+1/2} - 2\eta^{**}_{i+1/2,j+1/2} + \eta^{**}_{i-1/2,j+1/2}}{\Delta y(\Delta x)^2}\right]$$

$$- Bg \overset{-y}{h}{}^{3}_{i+1/2,j} \left[\frac{\overset{**}{\eta}_{i+3/2,j-1/2} - 2\overset{**}{\eta}_{i+1/2,j-1/2} + \overset{**}{\eta}_{i-1/2,j-1/2}}{\Delta x (\Delta y)^2} \right]$$

$$+ \frac{\overset{-y}{h}_{i+1/2,j} \left(h_{i+1/2,j+1/2} - h_{i+1/2,j-1/2} \right)}{\Delta t \Delta y} \left[\frac{1}{6} \frac{\left(Q^{n+3/2}_{i+1/2,j+1} - Q^{n+3/2}_{i+1/2,j+1} \right) - \left(Q^{n+1/2}_{i+1/2,j+1} - Q^{n+1/2}_{i+1/2,j-1} \right)}{\Delta y} \right]$$

$$+ \frac{\overset{-y}{h}_{i+1/2,j} \left(h_{i+1/2,j+1/2} - h_{i+1/2,j-1/2} \right)}{\Delta t \Delta y} \left[\frac{1}{6} \frac{\left(\overset{-y^{n+1}}{P}_{i+1,j} - \overset{-y^{n+1}}{P}_{i,j} \right) - \left(\overset{-y^{n}}{P}_{i+1,j} - \overset{-y^{n}}{P}_{i,j} \right)}{\Delta x} \right]$$

$$+ \frac{\overset{-x}{h}_{i+1/2,j} \left(\overset{=}{h}_{i+1,j} - \overset{=}{h}_{i,j} \right)}{\Delta t \Delta x} \left[\frac{1}{6} \frac{\left(\overset{-x^{n+1}}{P}_{i+1/2,j+1/2} - \overset{-x^{n+1}}{P}_{i+1/2,j-1/2} \right) - \left(\overset{-x^{n}}{P}_{i+1/2,j+1/2} - \overset{-x^{n}}{P}_{i+1/2,j-1/2} \right)}{\Delta y} \right]$$

$$+ Bg \overset{-y}{h}{}^{2}_{i+1/2,j} \left[2 \frac{\left(h_{i+1/2,j+1/2} - h_{i+1/2,j-1/2} \right)}{\Delta y} \frac{\left(\overset{-y^{**}}{\eta}_{i+1/2,j+1} - 2\overset{-y^{**}}{\eta}_{i+1/2,j} + \overset{-y^{**}}{\eta}_{i+1/2,j-1} \right)}{(\Delta y)^2} \right]$$

$$+ Bg \overset{-y}{h}{}^{2}_{i+1/2,j} \left[\frac{\left(h_{i+1/2,j+1/2} - h_{i+1/2,j-1/2} \right)}{\Delta y} \frac{\left(\overset{-y^{**}}{\eta}_{i+3/2,j} - 2\overset{-y^{**}}{\eta}_{i+1/2,j} + \overset{-y^{**}}{\eta}_{i-1/2,j} \right)}{(\Delta x)^2} \right]$$

$$+ Bg \overset{-y}{h}{}^{2}_{i+1/2,j} \left[2 \frac{\left(\overset{=}{h}_{i+1,j} - \overset{=}{h}_{i,j} \right)}{\Delta x} \frac{\left(\overset{-x^{**}}{\eta}_{i+1,j+1/2} - \overset{-x^{**}}{\eta}_{i,j+1/2} - \overset{-x^{**}}{\eta}_{i+1,j-1/2} + \overset{-x^{**}}{\eta}_{i,j-1/2} \right)}{\Delta x \Delta y} \right]$$

where

$$C^{y}_{Bhi} = \left(B + \frac{1}{3} \right) \frac{\overset{-y}{h}{}^{2}_{i+1/2,j}}{\Delta t}$$

$$D^{**}_{i+1/2,j} = \overset{-y}{h}_{i+1/2,j} + \overset{-y^{**}}{\eta}_{i+1/2,j}$$

$$D^{**}_{i+1/2,j+1/2} = h_{i+1/2,j+1/2} + \overset{**}{\eta}_{i+1/2,j+1/2}$$

$$D^{**}_{i+1/2,j-1/2} = h_{i+1/2,j-1/2} + \overset{**}{\eta}_{i+1/2,j-1/2}$$

$$D^{*}_{i+1,j} = \overset{=}{h}_{i+1,j} + \overset{=^{*}}{\eta}_{i+1,j}$$

$$D^{**}_{i,j} = \overset{=}{h}_{i,j} + \overset{=^{**}}{\eta}_{i,j}$$